CrystEngComm

ROYAL SOCIETY OF CHEMISTRY

PAPER

View Article Online
View Journal | View Issue

Cite this: *CrystEngComm*, 2025, **27**, 1541

Novel Ti@COF catalysts for the preparation of ultra-high molecular weight linear polyethylene†

Hao-Tian Li,‡[a] Jie Gu,‡[a] Nian-Zu Shu,[a] Guo-Long He,[a] He-Gen Zheng *[b] and Chuan-Lei Zhang *[a]

Received 13th January 2025,
Accepted 28th January 2025

DOI: 10.1039/d5ce00042d

rsc.li/crystengcomm

The development of the polyolefin industry hinges on the development of high-performance catalysts. Covalent organic frameworks (COFs), as novel porous materials, hold great potential in heterogeneous catalysis. In this study, Ti@COF catalysts, namely Ti@TbDa and Ti@TtDa, were designed and synthesized under solvothermal conditions and post-modification. Ethylene polymerization experiments demonstrated that Ti@TtDa exhibited an extremely high polymerization activity of 4.31×10^4 g_{PE} mol_{Ti}^{-1} h^{-1} at a pressure of 0.5 MPa, and the products have opened up new avenues for the production of ultra-high molecular weight linear polyethylene (M_w = 1.57×10^6 g mol^{-1}) and a low molecular weight distribution (D = 4.80). Such catalysts brought new ideas for the design of olefin polymerization catalysts and contributed to the upgrading of the polyethylene industry.

Introduction

Polyolefins, especially polyethylene, serve as the bedrock of modern industry, and the development of high-performance catalysts is pivotal to their industrial development.[1–3] Since the advent of Ziegler–Natta catalysts in the 1950s, the history of polyethylene catalysts has opened a new chapter.[4,5] This breakthrough not only significantly advanced ethylene polymerization technology but also laid a solid foundation for subsequent catalyst research.

The emergence of homogeneous catalysts such as earlier Ziegler–Natta catalysts, metallocene catalysts, and FI catalysts has played a crucial role in the development of the polyethylene industry. It has further propelled the vigorous development of the polyethylene industry and given rise to various types of polyethylene, such as high-density polyethylene (HDPE), low-density polyethylene (LDPE), and linear low-density polyethylene (LLDPE).[6–11] Homogeneous catalysts can fine-tune the molecular weight distribution and stereo-configuration of polymers, thereby enabling the production of polyethylene with tailored properties. However, these catalysts also have several notable drawbacks, such as the tendency of active centers to aggregate, difficulty in separation, and high production costs.

The development of heterogeneous catalysts effectively addresses the shortcomings of homogeneous catalysts. These catalysts are usually composed of homogeneous catalysts supported on solid carriers, such as silica or magnesium oxide.[12–16] Heterogeneous catalysts not only offer advantages such as stable active centers, ease of separation, and reusability, but they also have lower catalytic activity and broader molecular weight distributions of the polymers. Additionally, in most traditional heterogeneous solid catalysts, the active materials exhibit diverse properties, leading to complex interfacial effects. The impacts of individual active components and their interactions remain incompletely understood.

Covalent organic frameworks (COFs) are a new type of porous material assembled from organic structural units connected by covalent bonds, forming highly ordered and periodic network structures.[17–21] COFs possess abundant porous structures and high specific surface areas, which are advantageous for applications such as gas adsorption and separation.[22–24] By choosing different organic structural units and linking methods, the structures and properties of COFs can be flexibly tailored.[25,26] Furthermore, COFs can be functionalized by introducing functional groups or guest molecules, endowing them with properties such as catalysis, sensing, and energy storage, demonstrating broad application prospects, especially in the field of heterogeneous catalysis.[27–31] Compared to traditionally supported catalysts, the catalytic sites in Ti@COFs are confined within high-throughput one-

[a] *Anhui Provincial Key Laboratory of Advanced Catalysis and Energy Materials, Anhui Ultra High Molecular Weight Polyethylene Fiber Engineering Research Centre, School of Chemistry and Chemical Engineering, Anqing Normal University, Anqing 246133, China. E-mail: clzhang@nju.edu.cn*
[b] *State Key Laboratory of Coordination Chemistry, School of Chemistry and Chemical Engineering, Nanjing University, Nanjing 210023, China. E-mail: zhenghg@nju.edu.cn*

† Electronic supplementary information (ESI) available. See DOI: https://doi.org/10.1039/d5ce00042d

‡ These authors contributed equally to this work.

dimensional (1D) channels, which facilitates the ethylene polymerization reaction at these sites, thereby exhibiting excellent catalytic performance and efficiency in various catalytic transformations.[32–34] Liu *et al.*[35] immobilized the metallocene catalyst onto the COF framework through the bridging effect of methylaluminoxane (MAO), thereby enhancing the stability of the metallocene catalyst. Although it exhibits good catalytic activity, the molecular weight of the resulting polymer is relatively low ($M_w = 3.08 \times 10^5$ g mol^{-1}).

We designed and synthesized two structurally similar Ti@COF catalysts and applied them to ethylene polymerization reactions. Using a solvothermal method, the two monomers, 1,3,5-tri(4-aminophenyl)benzene (TAPB) and 2,4,6-tri(4-aminophenyl)-1,3,5-triazine (TAPT), were separately condensed with 2,5-dihydroxyterephthalaldehyde (DHA) to obtain TbDa and TtDa. These parent COFs were coordinated with $TiCl_4$ to prepare the two catalysts, Ti@TbDa and Ti@TtDa (see Scheme 1). And through ethylene polymerization experiments, the polymerization performance of Ti@COF catalysts and the characteristics of their polymerization products were verified.

Results and discussion

Amino monomers and aldehyde monomers underwent Schiff base condensation reactions to obtain highly crystalline COFs with imine–biphenyl units. Material Studio (MS) software was used to geometrically optimize the unit cells of model molecules, and the periodic crystal structure of the COF was determined through simulated powder X-ray diffraction (PXRD). The PXRD patterns of TbDa and TtDa exhibited the diffraction peaks required for COF formation, confirming the crystalline characteristics of these two COFs (Fig. 1a and b). The PXRD patterns of TbDa and TtDa showed intense peaks corresponding to the (100) plane at 2θ = 3.02° and 3.14°, respectively, and those at 4.99°/5.22°, 5.73°/5.80°, and 7.45°/7.68° correspond to the (110), (200), and (120) planes, respectively. In addition, the calculated PXRD spectra results of the AA stacking structures of the two COFs were consistent with the experimentally obtained peak positions and intensities. The calculated results of the Pawley-refined PXRD spectra were in agreement with the experimentally measured data, with both low residual factors and spectral differences (Tables S1 and S2, ESI†). The analysis results of powder X-ray diffraction (PXRD) (Fig. S7†) indicated that when Ti was coordinated with TtDa and TbDa, the obtained Ti@TtDa and Ti@TbDa retained their original crystal structures.

The synthesized TbDa and TtDa were further characterized using infrared spectroscopy (IR), confirming the presence of imine bonds in the COF structure. A new absorption peak corresponding to the characteristic vibration of the TtDa C=N bond was observed near 1625 cm^{-1}, and at the same time, the almost disappearance of the C=O stretching vibration bond (1670 cm^{-1}) and the N–H stretching vibration bonds (3317 and 3374 cm^{-1}) was detected (Fig. 1c), further confirming the successful synthesis of the COF. Nitrogen adsorption was employed to investigate the porosity of the parent COF and Ti@COF at 77 K. TbDa, TtDa, Ti@TbDa, and Ti@TtDa exhibited similar type II adsorption isotherms, and the calculated BET specific surface areas were 415.56, 873.83, 73.93, and 609.75 m^2 g^{-1} (Fig. 1d), respectively, with the pore

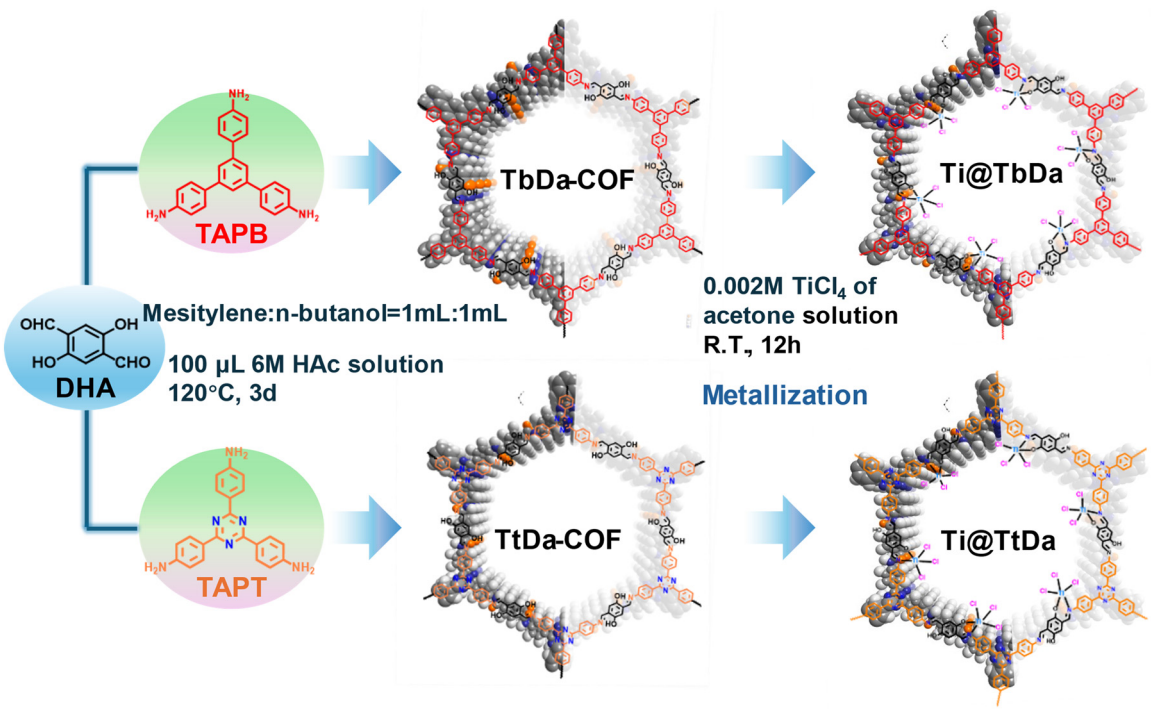

Scheme 1 Design and synthesis of the parent COF and Ti@COF.

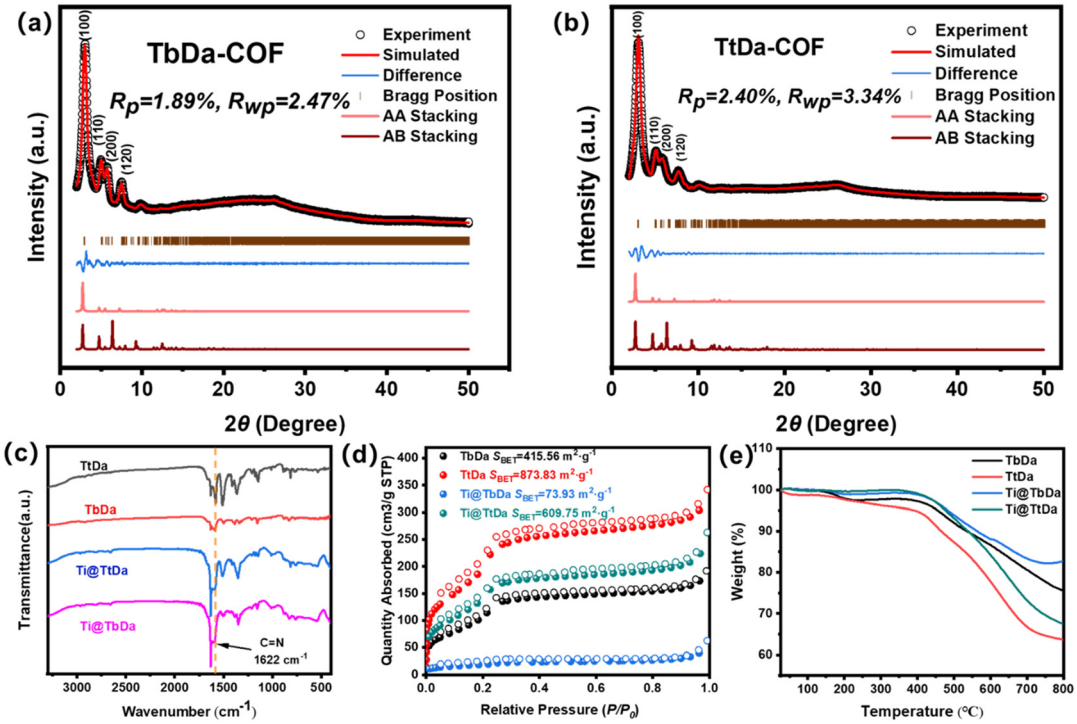

Fig. 1 The experimental and Pawley refined predicted powder X-ray diffraction (PXRD) patterns of TbDa (a) and TtDa (b); the infrared spectra of TbDa, TtDa, Ti@TbDa, and Ti@TtDa (c), the N_2 adsorption–desorption isotherms (d), and TGA curves under an N_2 atmosphere (e).

size mainly distributed in the range of 2 to 3 nm (Fig. S9†). This further confirmed that the two metallized COFs still maintained the AA stacking crystal framework. Furthermore, TGA analysis under an N_2 atmosphere showed that both the parent COF and Ti@COF maintained the integrity of the framework structure before 400 °C (Fig. 1e).

Further examination of the samples' morphologies using a scanning electron microscope (SEM) revealed that they consist of nanoscale particles with irregular shapes, rough surfaces, and porous characteristics, along with varying degrees of particle aggregation (Fig. 2a–d). Energy-dispersive X-ray spectroscopy (EDS) was performed on the two metallized Ti@COFs, and the results indicated that, in addition to C, N, and O elements, Ti and Cl elements were also uniformly distributed on the Ti@COF (Fig. 2e–j). Through ICP-AES analysis, we determined that the mass percentage contents of Ti in Ti@TbDa and Ti@TtDa were 4.11 wt% and 3.58 wt%, respectively.

To elucidate the elemental composition and chemical states on the material surfaces, X-ray photoelectron spectroscopy (XPS) was conducted on both the parent COF and the metallized Ti@COF. The analysis confirmed the presence of C, N, and O elements in the parent COF. In the Ti@COF samples, new binding energy peaks for Ti and Cl were observed (Fig. 3a). The high-resolution O 1s spectrum of the Ti@TtDa sample was deconvoluted into two peaks, with the peak at 530.27 eV

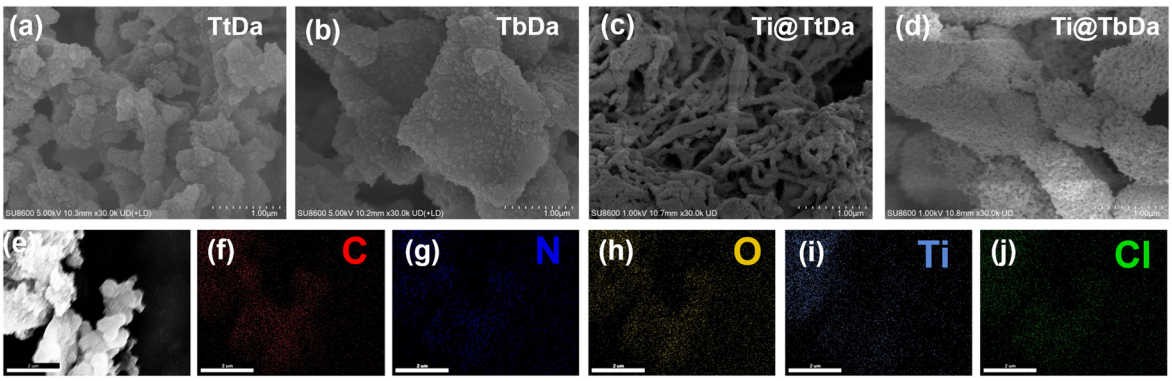

Fig. 2 SEM image of the parent COF and Ti@COF. SEM images of (a) TtDa, (b) TbDa, (c) Ti@TtDa, and (d) Ti@TbDa. (e)–(j) The EDX-mapping images of Ti@TtDa.

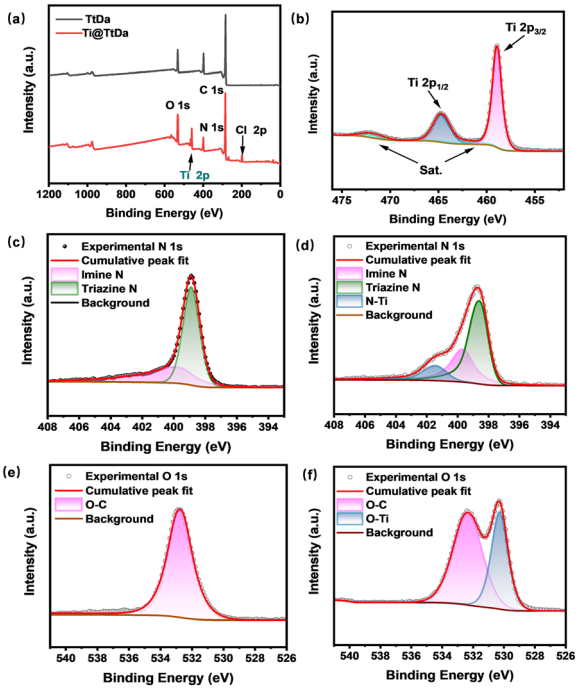

Fig. 3 XPS analysis of TtDa and Ti@TtDa. (a) Survey spectra of TtDa and Ti@TtDa; (b) high-resolution Ti 2p spectrum of Ti@TtDa; (c) high-resolution N 1s spectrum of TtDa; (d) high-resolution N 1s spectrum of Ti@TtDa; (e) high-resolution O 1s spectrum of TtDa; (f) high-resolution O 1s spectrum of Ti@TtDa.

assigned to the Ti–O bond (Fig. 3d) and the peak at 532.3 eV to the C–O bond. The high-resolution N 1s spectrum revealed three distinct nitrogen environments (Fig. 3f), corresponding to triazine nitrogen, imine nitrogen, and Ti–N bonds. The binding energies of Ti $2p_{1/2}$ and Ti $2p_{3/2}$ were approximately 464.66 eV and 458.89 eV, respectively (Fig. 3b), indicating the presence of Ti(IV)–O(N) in Ti@TtDa. Additionally, compared to TtDa, the C–O, imine, and triazine bonds in Ti@TtDa showed varying degrees of shift. Similarly, as depicted in Fig. S10,† Ti(IV)–O(N) was also detected in Ti@TbDa (Fig. S12†).

Polymerization experiments demonstrated that Ti@TtDa successfully synthesized ultra-high molecular weight polyethylene with a molecular weight of 1.57×10^6 g mol^{-1} at 0.5 MPa pressure, and a relatively narrow molecular weight distribution (polydispersity index D = 4.8). Compared to Ti@TbDa, the catalytic activity of Ti@TtDa was significantly enhanced, nearly doubled. The activity of Ti@TbDa increased linearly with pressure, while its molecular weight remained relatively stable under different pressures (1.42×10^6 g mol^{-1} at 0.5 MPa, 1.35×10^6 g mol^{-1} at 1.0 MPa, and 1.41×10^6 g mol^{-1} at 1.5 MPa). Fig. S13 and S14† show that both types of polyethylene exhibit good linearity at 5 bar pressure. We speculate that the triazine ring structure in Ti@TtDa provides a nitrogen-rich hydrogen bonding microenvironment for ethylene molecules, facilitating the enrichment of ethylene around the metal active sites, thereby promoting the coordination of ethylene and the growth of the polyethylene chain. In the ethylene polymerization catalyzed by the Ti@COF, hydrogen bonds play a crucial role under low-pressure conditions, maintaining high catalytic activity and resulting in polymers with the highest molecular weight and the narrowest molecular weight distribution. However, under high-pressure conditions (≥1.0 MPa), the influence of hydrogen bonds weakens, leading to a decrease in the polymer molecular weight and an increase in the molecular weight distribution. Under these conditions, the catalytic performance of Ti@TtDa and Ti@TbDa is comparable.

High temperatures typically enhance reaction kinetics; however, homogeneous catalysts like metallocene complexes tend to lose their catalytic efficiency rapidly or become entirely inactive when the temperature reaches 70–80 °C.[36–38] In contrast, the Ti@COF catalysts maintain significant catalytic activity even at high temperatures of up to 100 °C, which is likely attributed to the high thermal stability of the COF framework. To assess the performance of the Ti@COF catalysts, we conducted a series of polymerization tests under 100 °C using various ethylene pressures, and the results are systematically displayed in Table 1. Subsequent analysis using differential scanning calorimetry (DSC) and gel permeation chromatography (GPC) indicated that the polymers produced by the Ti@COF catalysts exhibit high melting points, ultra-high molecular weights, and excellent linearity. We speculate that the high crystallinity and the highly oriented one-dimensional channels of the COF structure may play a role in controlling the

Table 1 Summary of ethylene polymerization experiments with Ti@COF catalysts

Ent.	Cat.[a]	P (MPa)	Activity[b] (10^4)	M_w[c] (10^6)	M_n[c] (10^5)	D[c]	T_m[d] (°C)
1	Ti@TtDa	0.5	4.31	1.57	3.28	4.80	133.25
2	Ti@TtDa	1.0	6.16	1.44	4.59	3.20	132.89
3	Ti@TtDa	1.5	8.99	1.46	4.33	3.40	132.88
4	Ti@TbDa	0.5	2.39	1.42	3.98	3.60	134.12
5	Ti@TbDa	1.0	6.12	1.35	4.17	3.20	133.59
6	Ti@TbDa	1.5	8.56	1.41	3.35	4.20	132.38

[a] Polymerization conditions: the polymerization was conducted using MAO as a cocatalyst with an Al/Ti molar ratio of 1500 mol mol^{-1}, 10 mg of the Ti@COF catalyst, and 30 mL of toluene as the solvent at 100 °C for 1 hour. [b] Activity unit: the activity is expressed as the mass of ethylene polymerized per mole of titanium per hour (g_{PE} mol_{Ti}^{-1} h^{-1}). [c] Molecular weight data: the weight-average molecular weight (M_w), number-average molecular weight (M_n), and polydispersity index (D) were determined by high-temperature gel permeation chromatography (GPC). [d] Melting characteristics: the melting peak temperature (T_m) was assessed by differential scanning calorimetry (DSC, second heating).

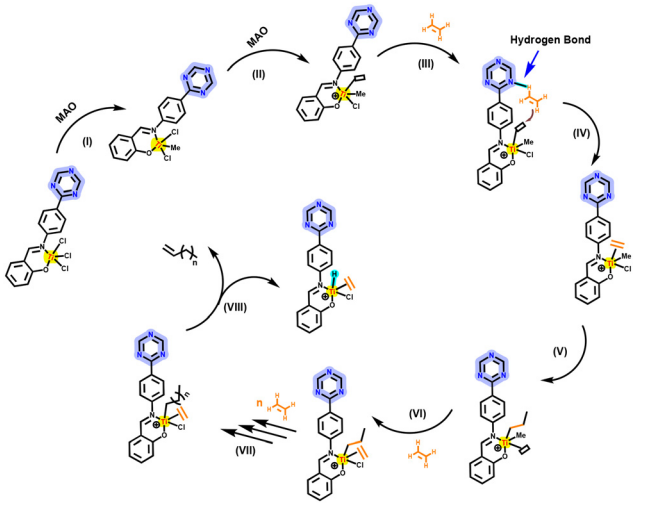

Scheme 2 Ti@TtDa ethylene polymerization mechanism under a low ethylene pressure (note: steps I to III are the chain initiation processes, steps IV to VII are the chain growth processes, and step VIII is the chain termination process).

β-H elimination during polymerization, thereby restricting the degree of polymer branching and promoting the formation of ultra-high molecular weight linear polyethylene.[39]

In general, the ethylene polymerization process can be divided into three main stages: cocatalyst activation (chain initiation), chain growth, and chain termination. As depicted in Scheme 2, the active species in the ethylene polymerization involving Ti@TtDa is the ligand-stabilized, ligand-unsaturated cationic alkyl complex M^+. Starting from the Ti metal halide precursor, the combination of alkylation and alkyl removal steps leads to the production of polyethylene, with MAO facilitating the simultaneous alkylation and alkyl removal steps of the Ti metal halide. Once the active species M^+ is formed, ethylene coordination and insertion occur at the unsaturated Ti coordination site. The alkyl group migrates and inserts into the ethylene, forming a new alkyl chain that grows by two carbon atoms and creating a new unsaturated ligand Ti site,[40] a process known as chain growth. The N atom of the triazine ring, bearing a lone pair of electrons, can form hydrogen bonds to enhance the enrichment of ethylene around the metal site, facilitating the coordination of ethylene with the metal active site and the subsequent growth of the PE chain. During chain termination, β-H migration generates vinyl-bearing compounds and Ti–H species, which can reinsert into a monomer and then re-emerge as the center of chain growth.

Conclusions

This study successfully constructs and characterizes two innovative Ti@COF catalysts, which are effectively applied in ethylene polymerization reactions. In Ti@TtDa, the triazine ring containing nitrogen atoms and lone pairs of electrons can efficiently gather ethylene molecules around the metal active sites, thereby promoting the formation of metal–π bonds and the extension of polyethylene chains. As a novel heterogeneous catalytic system, Ti@TtDa can efficiently synthesize high molecular weight linear polyethylene (with a molecular weight M_w of 1.57×10^6 g mol^{-1}) under a low ethylene partial pressure (0.5 MPa), demonstrating extremely high catalytic activity (4.31×10^4 g_{PE} mol_{Ti}^{-1} h^{-1}). Ethylene polymerization under low-pressure conditions heralds significant potential in the expansion of the polyethylene industry, while the synthesis of high-activity and ultra-high molecular weight polyethylene marks a major advancement in the polyethylene industry. Moreover, the excellent polymerization capabilities of Ti@TtDa open up new ideas and methods for the design and synthesis of catalysts in the field of heterogeneous olefin polymerization.

Experimental sections

Ethylene polymerization experiment

The polymerization process takes place in a 250 mL stainless steel high-pressure reactor fitted with a mechanical stirrer as well as systems for controlling the pressure and temperature, at a predetermined ethylene pressure. To begin with, the reactor is subjected to high-temperature baking in a vacuum environment for a duration of 12 hours, after which the internal gas is purged and replaced with nitrogen in three separate cycles. Once the reactor reaches a temperature of 100 °C, 30 mL of the toluene solvent that has been dried using a molecular sieve is introduced. Upon the temperature reaching 100 °C again, the requisite quantity of the cocatalyst (MAO) is incorporated, and 10 mg of the Ti@COF catalyst is suspended in 5 mL of toluene *via* ultrasonication to ensure uniform dispersion. Following 5 minutes of stirring, the reactor is pressurized to the target ethylene pressure level and agitated intensely at a rate of 1000 revolutions per minute. Once the reaction has proceeded for 1 hour, the heating is halted and the ethylene pressure is vented. The reaction mixture is subsequently quenched using a solution of 10% hydrochloric acid in ethanol. The resultant polymer is then harvested, rinsed with ethanol, and finally dried in a vacuum at 100 °C.

Synthesis of TbDa–COF

A 15 mL Schlenk flask (OD 26 × *L* 70 mm) was charged with the following reagents: 1,3,5-tris(4-aminophenyl)benzene (14.1 mg, 0.04 mmol), 2,5-dihydroxyterephthalaldehyde (10 mg, 0.06 mmol), mesitylene (1 mL), and *n*-butanol (1 mL). The assembly was subjected to ultrasonic treatment for 10 minutes. Following the ultrasonication, a 6 M aqueous solution of acetic acid (100 μL) was gradually added to the mixture. The contents were then degassed through a series of freeze–pump–thaw cycles to remove any dissolved gases. After degassing, the Schlenk flask was sealed and maintained at a constant temperature of 120 °C for 3 days. Upon cooling to ambient temperature, a reddish-brown product was isolated by filtration and subsequently washed three times with acetone. The damp product was then transferred to a Soxhlet extractor and washed with dioxane for 24 hours, followed by

a period of washing with THF. The solid was placed in a vacuum oven to dry, yielding a yellow-brown COF product weighing 17.3 mg with a yield of 78.85%.

Synthesis of the TtDa–COF

The synthesis of TtDa follows a similar procedure to that of TbDa, but with the use of the precursor 2,4,6-tris(4-aminophenyl)-1,3,5-triazine (14.2 mg, 0.04 mmol) instead of 1,3,5-tris(4-aminophenyl)benzene. This precursor is combined with 2,5-dihydroxyterephthalaldehyde (10 mg, 0.06 mmol), mesitylene (1 mL), and *n*-butanol (1 mL) in a 15 mL Schlenk tube (OD 26 × *L* 70 mm). The mixture is then subjected to 10 minutes of ultrasonic treatment to ensure thorough mixing of the reagents. After ultrasonication, 6 M aqueous acetic acid (100 μL) is gradually added to the mixture, followed by a series of freeze–pump–thaw cycles to degas the contents and remove any dissolved gases. Once degassing is complete, the Schlenk tube is sealed and maintained at 120 °C for 3 days. After the reaction, the system is allowed to cool to room temperature, and a reddish-brown TtDa product is isolated by filtration and washed 3 times with acetone to remove the residual solvents. The damp TtDa product is then transferred to a Soxhlet extraction apparatus, initially washed with dioxane for 24 hours, followed by further washing with THF. Finally, the solid product is dried in a vacuum oven to yield yellow-brown TtDa, with a mass of 17.9 mg and a yield of 81.54%.

Synthesis of the Ti@COF catalyst

Commenced by weighing out 20.0 milligrams of TbDa and TtDa each and then placing them into separate vials. Thereafter, 3.8 μL of titanium tetrachloride ($TiCl_4$, 0.02 mmol) is added, which had been pre-dissolved in 10.0 mL of acetone, to each vial. The mixtures are subjected to slow stirring over a period of 12 hours at room temperature to ensure a complete reaction. Post-reaction, the dark brown-black solid products are collected *via* filtration and washed with acetone 4 to 5 times to remove any residual Ti metal. The solids are then transferred to a Soxhlet extractor for further purification with acetone over 12 hours. The final step involves drying the products under vacuum to yield the two types of Ti@COF catalysts. Prior to conducting polymerization experiments, the prepared catalysts are activated by treating them under a vacuum of 10^{-2} mTorr at 170 °C for 12 hours.

Data availability

All data supporting the findings of this study are available within the manuscript and its ESI.†

Author contributions

Hao-Tian Li: investigation, validation, formal analysis, data curation, and writing – original draft. Jie Gu: data curation and writing – original draft. Nian-Zu Shu: data curation and formal analysis. Guo-Long He: software – supporting and visualization. He-Gen Zheng: data curation. Chuan-Lei Zhang: writing – review & editing, funding acquisition, and supervision.

Conflicts of interest

There are no conflicts to declare.

Acknowledgements

This work was supported by grants from the National Natural Science Foundation of China (No. 22101006 and 21771101), the Natural Science Research Major Project of Anhui Provincial Department of Education (2023AH040071), the Key Project for Cultivating Outstanding Young Teachers in Universities of Anhui Province (YQZD2023058) and Anhui Natural Science Foundation Youth Project (No. 1908085QB49).

References

1 H. Deng, H. Zheng, H. Gao, L. Pei and H. Gao, *Catalysts*, 2022, **12**, 936.
2 Q. Mahmood, X. Li, L. Qin, L. Wang and W.-H. Sun, *Dalton Trans.*, 2022, **51**, 14375–14407.
3 Y. Wang, J. Lai, R. Gao, Q. Gou, B. Li, G. Zheng, R. Zhang, Q. Yue, Z. Song and Z. Guo, *Polymers*, 2024, **16**, 1676.
4 V. Busico, R. Cipullo, R. Pellecchia, S. Ronca, G. Roviello and G. Talarico, *Proc. Natl. Acad. Sci. U. S. A*, 2006, **103**, 15321–15326.
5 T. Pongchan, P. Praserthdam and B. Jongsomjit, *Mater. Today Chem.*, 2020, **18**, 100366.
6 C. Li, G. Fan, G. Zheng, R. Gao and L. Liu, *Polymers*, 2024, **16**, 2717.
7 C. Bariashir, C. Huang, G. A. Solan and W.-H. Sun, *Coord. Chem. Rev.*, 2019, **385**, 208–229.
8 M. Stasiak, A. Studer, A. Greiner and J. H. Wendorff, *Chem. – Eur. J.*, 2007, **13**, 6150–6156.
9 Y.-L. Sun, Y.-H. Hou, M.-M. Cui, H. Meng, B.-Y. Liu and M. Yang, *Catal. Lett.*, 2024, **154**, 1945–1957.
10 A. Köllhofer and H. Plenio, *Chem. – Eur. J.*, 2003, **9**, 1416–1425.
11 S. H. Cho, I. Pelczer and R. A. Register, *Macromolecules*, 2021, **54**, 10300–10311.
12 Z. Ma, M. Xu, N. Zhu, C. Tan and C. Chen, *Chin. J. Chem.*, 2023, **41**, 1155–1162.
13 D. E. Ortega, L. Gracia and D. Cortés-Arriagada, *Mol. Catal.*, 2023, **549**, 113509.
14 Q. Wang, W. Wang, W. Qu, W. Pang, M. Qasim and C. Zou, *J. Polym. Sci.*, 2023, **61**, 115–122.
15 H. Zhang, Z. Zhang, Z. Cai, M. Li and Z. Liu, *ACS Catal.*, 2022, **12**, 9646–9654.
16 Y. Teng, D. Liu, Q. Li, X. Bai and Y. Song, *Catalysts*, 2023, **13**, 236.
17 H. Bhambri, S. Khullar, Sakshi and S. K. Mandal, *Mater. Adv.*, 2022, **3**, 19–124.
18 A. Laemont, G. Matthys, R. Lavendomme and P. Van Der Voort, *Angew. Chem., Int. Ed.*, 2024, **63**, e202412420.

19 H. R. Abuzeid, A. F. M. El-Mahdy and S.-W. Kuo, *Giant*, 2021, **6**, 100054.
20 Q. Fang, Z. Zhuang, S. Gu, R. B. Kaspar, J. Zheng, J. Wang, S. Qiu and Y. Yan, *Nat. Commun.*, 2014, **5**, 4503.
21 K. T. Tan, S. Ghosh, Z. Wang, F. Wen, D. Rodríguez-San-Miguel, J. Feng, N. Huang, W. Wang, F. Zamora, X. Feng, A. Thomas and D. Jiang, *Nat. Rev. Methods Primers*, 2023, **3**, 1.
22 X. Wang, M. Liu, Y. Liu, S. Shang, C. Du, J. Hong, W. Gao, C. Hua, H. Xu, Z. You, J. Chen and Y. Liu, *J. Am. Chem. Soc.*, 2023, **145**, 26900–26907.
23 M.-X. Wu and Y.-W. Yang, *Chin. Chem. Lett.*, 2017, **28**, 1135–1143.
24 X. Ma, N. Sun, Z. Li, M. Tong, Q. Ding, Z. Wang, L. Bai, L. Dong and Y. Liu, *Adv. Funct. Mater.*, 2024, **34**, 2312203.
25 W. Wu, Z. Li, S. Liu, D. Zhang, B. Cai, Y. Liang, M. Wu, Y. Liao and X. Zhao, *Angew. Chem., Int. Ed.*, 2024, **63**, e202404563.
26 J. Du, Y. Liu, R. Krishna, Y. Yu, Y. Cui, S. Wang, Y. Liu, X. Song and Z. Liang, *ACS Appl. Mater. Interfaces*, 2018, **10**, 26678–26686.
27 Y. Yin, Y. Zhang, X. Zhou, B. Gui, W. Wang, W. Jiang, Y.-B. Zhang, J. Sun and C. Wang, *Science*, 2024, **386**, 693–696.
28 L. Peng, S. Yang, S. Jawahery, S. M. Moosavi, A. J. Huckaba, M. Asgari, E. Oveisi, M. K. Nazeeruddin, B. Smit and W. L. Queen, *J. Am. Chem. Soc.*, 2019, **141**, 12397–12405.
29 H. Sun, Z. Wu, T. Xia, Y. Zhao, Y. Li, L. Shan, C. Li, Z. Sui, R. Fan and Q. Chen, *Mater. Lett.*, 2022, **327**, 133065.
30 Y. Bian, X. Song, Y. Han, G. Wang and H. Qiao, *Tetrahedron Lett.*, 2024, **150**, 155281.
31 Z. Alsudairy, N. Brown, A. Campbell, A. Ambus, B. Brown, K. Smith-Petty and X. Li, *Mater. Chem. Front.*, 2023, **7**, 3298–3331.
32 H. Zheng and S. Che, *Natl. Sci. Rev.*, 2024, **11**, nwae172.
33 L. Song, W. Gao, S. Jiang, Y. Yang, W. Chu, X. Cao, B. Sun, L. Cui and C.-y. Zhang, *Nano Lett.*, 2024, **24**, 6312–6319.
34 F. Jin, E. Lin, T. Wang, S. Geng, T. Wang, W. Liu, F. Xiong, Z. Wang, Y. Chen, P. Cheng and Z. Zhang, *J. Am. Chem. Soc.*, 2022, **144**, 5643–5652.
35 B. Zhu, K. Liu, L. Luo, Z. Zhang, Y. Xiao, M. Sun, S. Jie, W.-J. Wang, J. Hu, S. Shi, Q. Wang, B.-G. Li and P. Liu, *Chem. – Eur. J.*, 2023, **29**, e202300913.
36 S. Al-Malaika, U. Daraz and S. Issenhuth, *J. Vinyl Addit. Technol.*, 2022, **28**, 254–273.
37 J. Zhang, X. Wang and G.-X. Jin, *Coord. Chem. Rev.*, 2006, **250**, 95–109.
38 J. Moreno, B. Paredes, A. Carrero and D. Vélez, *Chem. Eng. J.*, 2017, **315**, 46–57.
39 H.-T. Li, T. Zhou, Y.-Q. Peng, X.-K. Shi, Z.-H. Zhu, Y.-B. Guan, Y.-Q. Li, Z. Liu and C.-L. Zhang, *J. Mater. Chem. A*, 2024, **12**, 32845–32854.
40 M. Brookhart, A. F. Volpe, Jr., D. M. Lincoln, I. T. Horvath and J. M. Millar, *J. Am. Chem. Soc.*, 1990, **112**, 5634–5636.